

Supplemental material

I. $7p\ ^2P_{1/2}^o$ STATE BRANCHING FRACTION SYSTEMATICS

A. Residual birefringence and the Hanle effect

If the light driving the $S_{1/2} \rightarrow P_{1/2}$ or the $D_{3/2} \rightarrow P_{1/2}$ transitions has a circularly polarized component, there will be an imbalance between right- and left-handed circularly polarized photons that are spontaneously emitted by the radium ion due to the Hanle effect [1–3]. Residual birefringence in the imaging system could result in different detection efficiencies for the two circular polarizations which would shift the branching fraction result. We used the technique developed with Ca^+ to bound our uncertainty due to residual birefringence [4]. We reversed the magnetic field direction, so any imbalance between the number of right- and left-handed circularly polarized photons detected would be reversed [2]. The measured branching fraction to the $S_{1/2}$ state with the magnetic field reversed, 0.9107(5), agrees with the measured branching fraction with the original magnetic field direction, 0.9104(5), within the statistical uncertainty. Therefore residual birefringence in the imaging system contributes at most at the level of the measurement’s statistical uncertainty, and so we set the systematic uncertainty to the statistical uncertainty, 5×10^{-4} .

B. PMT dead time

Photon pile-up at the PMT is a source of under counting. The PMT (Hamamatsu H10682-210) has a dead time of 20 ns [5], and we conservatively estimate the dead time uncertainty to be the same as the dead time, 20 ns. We calculate a PMT dead time compensated count rate from the measured count rate with

$$N = \frac{N_m}{1 - N_m t_d} \quad (\text{S1})$$

where N is the PMT dead time compensated count rate, N_m is the measured count rate, and t_d is the PMT dead time. The measured count rate is calculated from binned counts in Fig 2 in the main text. The systematic shift of the branching fraction to the $S_{1/2}$ state is the difference between the two branching fractions calculated with the PMT dead time compensated counts and the measured counts respectively, which gives $3(3) \times 10^{-6}$.

C. Collisions

Background gas collisions may knock the ion out of the imaging region, leading to varying detection efficiencies during the experiment. Collisions may also pump an ion to the $D_{5/2}$ state from the $D_{3/2}$ state.

We use the experiment sequence shown in Fig. S1 to determine the collision rate. A 160 ms long Doppler cooling pulse is first applied. After cooling, the ion is pumped to the $D_{3/2}$ state by a 468 nm pulse. Then there is a wait time of 160 ms before the cycle repeats. During the experiment the fluorescence counts at 468 nm are time-tagged in 10 ms bins. We identify collisions during the 160 ms wait time based on the fluorescence at the start of laser cooling. If

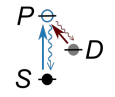
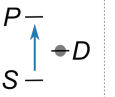
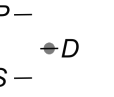
	cooling	pump	wait
468 nm			
1079 nm			
time	160 ms	50 μ s	160 ms
ion state			

FIG. S1. Pulse sequence and corresponding ion states for the collision rate measurement.

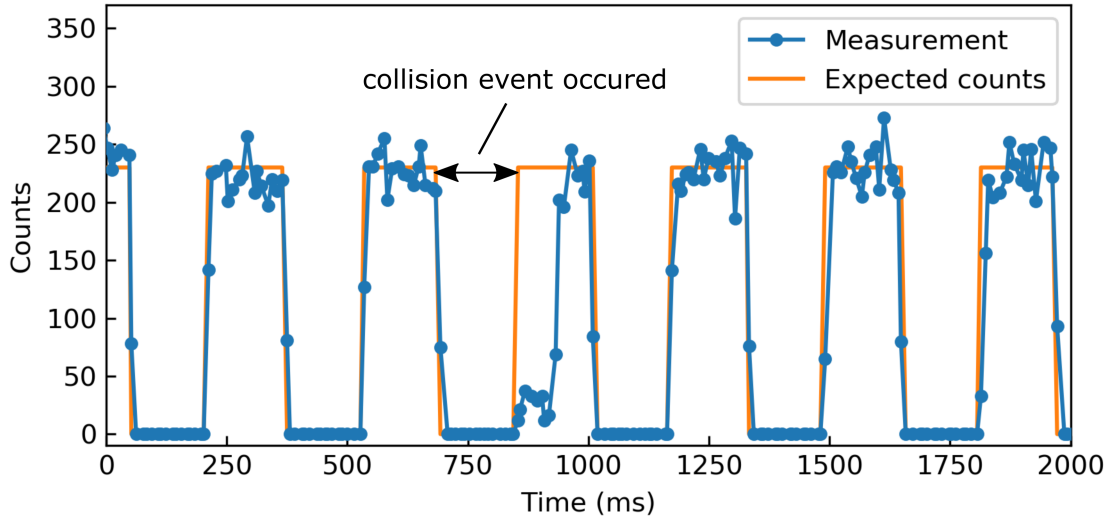


FIG. S2. A subset (1%) of our collision measurement data, where a collision occurred between 690 ms and 850 ms while the ion was not illuminated with light.

the fluorescence rapidly saturates, there was no collision. If the fluorescence recovers slowly, we conclude there was a collision, as shown in Fig. S2.

Due to the long lifetime of the $D_{3/2}$ state compared to the 160 ms long wait time, the ion stays in the $D_{3/2}$ state for the majority of the wait time, which increases the probability to see fine structure mixing during collisions. Once a fine structure mixing collision happens, the long lifetime of the $D_{5/2}$ state ensures that the ion is more likely to stay in the $D_{5/2}$ state during Doppler cooling.

From the collision experiment, we derive a collision rate of 0.26(6) Hz. We consider the worst case scenario where all collision events shift the branching fraction result to one direction. Using a collision rate of 0.32 Hz (84% confidence), the upper bound on the branching fraction systematic uncertainty due to collisions is 4×10^{-5} .

D. Optical Bloch equation simulations

We modelled the optical Bloch equations (OBE) of the Ra^+ lambda system using Mathematica’s “AtomicDensityMatrix” package [6] to calculate the $P_{1/2}$ state branching fraction systematics due to the finite measurement time,

the $D_{3/2}$ state lifetime, and finite AOM extinction ratios. The optical Bloch equations are:

$$\begin{aligned}
\rho'_{1,1}(t) &= \Gamma_P \rho_{3,3}(t) + \Gamma_D \rho_{2,2}(t) - \frac{i}{2} \Omega_{SP} [\rho_{1,3}(t) - \rho_{3,1}(t)] \\
\rho'_{1,2}(t) &= -i[(\Delta_{SP} - \Delta_{DP}) \rho_{1,2}(t) + \frac{1}{2} \Omega_{DP} \rho_{1,3}(t) - \frac{1}{2} \Omega_{SP} \rho_{3,2}(t)] \\
\rho'_{1,3}(t) &= -\frac{1}{2} \Gamma_P \rho_{1,3}(t) - i\{\Delta_{SP} \rho_{1,3}(t) + \frac{1}{2} \Omega_{DP} \rho_{1,2}(t) + \frac{1}{2} \Omega_{SP} [\rho_{1,1}(t) - \rho_{3,3}(t)]\} \\
\rho'_{2,1}(t) &= -i[(\Delta_{DP} - \Delta_{SP}) \rho_{2,1}(t) - \frac{1}{2} \Omega_{DP} \rho_{3,1}(t) + \frac{1}{2} \Omega_{SP} \rho_{2,3}(t)] \\
\rho'_{2,2}(t) &= \Gamma_P (1-p) \rho_{3,3}(t) - \Gamma_D \rho_{2,2}(t) - \frac{i}{2} \Omega_{DP} [\rho_{2,3}(t) - \rho_{3,2}(t)] \\
\rho'_{2,3}(t) &= -\frac{1}{2} \Gamma_P \rho_{2,3}(t) - i\{\Delta_{DP} \rho_{2,3}(t) + \frac{1}{2} \Omega_{SP} \rho_{2,1}(t) + \frac{1}{2} \Omega_{DP} [\rho_{2,2}(t) - \rho_{3,3}(t)]\} \\
\rho'_{3,1}(t) &= -\frac{1}{2} \Gamma_P \rho_{3,1}(t) - i\{-\Delta_{SP} \rho_{3,1}(t) - \frac{1}{2} \Omega_{DP} \rho_{2,1}(t) - \frac{1}{2} \Omega_{SP} [\rho_{1,1}(t) - \rho_{3,3}(t)]\} \\
\rho'_{3,2}(t) &= -\frac{1}{2} \Gamma_P \rho_{3,2}(t) - i\{-\Delta_{DP} \rho_{3,2}(t) - \frac{1}{2} \Omega_{SP} \rho_{1,2}(t) - \frac{1}{2} \Omega_{DP} [\rho_{2,2}(t) - \rho_{3,3}(t)]\} \\
\rho'_{3,3}(t) &= -\Gamma_P \rho_{3,3}(t) - i\{-\frac{1}{2} \Omega_{DP} (\rho_{2,3} - \rho_{3,2}) - \frac{1}{2} \Omega_{SP} [\rho_{1,3}(t) - \rho_{3,1}(t)]\}
\end{aligned} \tag{S2}$$

where $\rho_{i,j}$ are the density matrix elements, and subscripts i and j denote the $S_{1/2}$ (1), $D_{3/2}$ (2) and $P_{1/2}$ (3) states. The natural linewidth of the $P_{1/2}$ ($D_{3/2}$) state is Γ_P (Γ_D). The branching fraction of $P_{1/2}$ to $S_{1/2}$ is p . The detuning of the 468 nm (1079 nm) laser is Δ_{SP} (Δ_{DP}), with Rabi frequency Ω_{SP} (Ω_{DP}).

The best available linewidth values are the theoretically calculated values $\Gamma_P = 2\pi \times 18.6(2)$ MHz [7] and $\Gamma_D = 2\pi \times 1.57(2)$ Hz [8]. For the branching fraction we use our statistical result, $p = 0.9104$. We estimate that the detunings of the lasers $\Delta_{SP} = 0$ and $\Delta_{DP} = 2\pi \times 20$ MHz from linescan measurements.

The time-dependence of the Rabi frequencies, Ω_{SP} and Ω_{DP} , is determined by the pulse sequence shown in Fig. 2 of the main text. By fitting photon counts in N_b^F and N_r^F with the $P_{1/2}$ state population in the simulation, $\rho_{3,3}$, we determined the Rabi frequencies when a laser is on, $\Omega_{SP}^{\text{on}} = 2\pi \times 4.5$ MHz and $\Omega_{DP}^{\text{on}} = 2\pi \times 6.7$ MHz. A 10% uncertainty for the Rabi frequencies accounts for laser intensity fluctuations during measurement. When a laser is off, the Rabi frequency is set to 0 unless otherwise noted.

The initial condition for the simulations is $\rho_{1,1} = 1$, and all other $\rho_{i,j} = 0$. We numerically integrate $\rho_{3,3}$ during the time span of each 468 nm or 1079 nm laser pulse to calculate I_B^F , I_B^B , I_R^F , and I_R^B , where the same notation to denote photon counts is used as in the main text. The branching fraction from the simulation is calculated with

$$p_{\text{sim}} = \frac{I_B^F - I_B^B}{(I_B^F - I_B^B) + (I_R^F - I_R^B)}. \tag{S3}$$

We determine the systematic shift and uncertainty due to the finite measurement time with an OBE simulation where Γ_D is infinity, and Ω_{SP}^{off} and Ω_{DP}^{off} are 0. We compare the branching fraction calculated from the simulation, p_{sim}^f , to the branching fraction $p = 0.9104$ used as the simulation input, and it gives 5×10^{-9} shift and 3×10^{-7} uncertainty.

The $D_{3/2}$ state lifetime systematic is simulated with the same parameters as the finite measurement time OBE simulation except Γ_D is set to the theoretically calculated value. The difference of the branching fractions from the two simulations, p_{sim}^D and p_{sim}^f , give a shift of 2×10^{-7} and an uncertainty of 2×10^{-8} due to the $D_{3/2}$ state lifetime.

We use the OBEs to calculate the systematic uncertainty due to finite AOM extinction ratios. We measured that the light intensity extinction ratios of the 468 nm and 1079 nm AOMs are both greater than 60 dB using a PMT for the 468 nm light, and a photodiode for the 1079 nm light, corresponding to at least 30 dB suppression in Rabi frequency. We ran three OBE simulations with (a) $\Omega_{SP}^{\text{off}} = 10^{-3} \Omega_{SP}^{\text{on}}$ and $\Omega_{DP}^{\text{off}} = 0$, (b) $\Omega_{SP}^{\text{off}} = 0$ and $\Omega_{DP}^{\text{off}} = 10^{-3} \Omega_{DP}^{\text{on}}$, and (c) $\Omega_{SP}^{\text{off}} = 10^{-3} \Omega_{SP}^{\text{on}}$ and $\Omega_{DP}^{\text{off}} = 10^{-3} \Omega_{DP}^{\text{on}}$. Other simulation parameters are identical to the $D_{3/2}$ lifetime OBE simulation. The systematic uncertainty due to the finite AOM extinction ratios is bounded by the maximum shift of branching fractions simulated with finite AOM extinction ratios (a), (b), (c), from p_{sim}^D , which is 5×10^{-7} .

II. ESTIMATION OF EXCESS MICROMOTION BROADENING SYSTEMATICS ON THE $S_{1/2} \rightarrow P_{1/2}$ LINESCAN MEASUREMENT

Excess micromotion broadens the measured linewidth of the $P_{1/2}$ state due to the Doppler effect. We compensate micromotion in our trap by applying DC voltages to the trap's four radial electrodes. We optimized the bias voltages by minimizing displacement of an ion while varying the RF trapping amplitude. The ion position is monitored with a camera. We estimate that the residual stray field at the trap center is about 2 V/m, which is not compensated further due to the finite step size of the bias voltages. The 468 nm micromotion modulation index is about 1.8 for $^{226}\text{Ra}^+$ ions at Mathieu $q \sim 0.15$, corresponding to a broadening of about 2.1 MHz from Eqs. 22 and 28 of [9].

-
- [1] A. Gallagher and A. Lurio, Phys. Rev. Lett. **10**, 25 (1963).
 - [2] D. Zimmermann, Zeitschrift für Physik A Atoms and Nuclei **275**, 5 (1975).
 - [3] T. Pruttivarasin, *Spectroscopy, fundamental symmetry tests and quantum simulation with trapped interactions*, Ph.D. thesis, University of California, Berkeley (2014).
 - [4] M. Ramm, T. Pruttivarasin, M. Kokish, I. Talukdar, and H. Häffner, Phys. Rev. Lett. **111**, 023004 (2013).
 - [5] *Photon counting heads H10682 series*, Hamamatsu (2016).
 - [6] <http://rochesterscientific.com/ADM/>.
 - [7] B. K. Sahoo, L. W. Wansbeek, K. Jungmann, and R. G. E. Timmermans, Phys. Rev. A **79**, 052512 (2009).
 - [8] R. Pal, D. Jiang, M. S. Safronova, and U. I. Safronova, Phys. Rev. A **79**, 062505 (2009).
 - [9] D. J. Berkeland, J. D. Miller, J. C. Bergquist, W. M. Itano, and D. J. Wineland, J. Appl. Phys. **83**, 5025 (1998).